Z. Angew. Math. Phys. 64 (2013), 863–883
© 2012 Springer Basel AG
0044-2275/13/030863-21
published online June 19, 2012
DOI 10.1007/s00033-012-0237-5

Zeitschrift für angewandte Mathematik und Physik ZAMP

Semi-analytical approximations for a class of multi-parameter eigenvalue problems related to tensile buckling

Ciprian D. Coman and Xiang Liu

Abstract. This work complements the first author's recent asymptotic investigations on a class of boundary-eigenvalue problems for tensile buckling of thin elastic plates. In particular, it is shown here that the approximations for the critical buckling load can be improved by using a modified energy method that relies directly on the asymptotic results derived previously. We also explore a number of additional mathematical features that have an intrinsic interest in the context of multi-parameter eigenvalue problems.

Mathematics Subject Classification. 74K20, 74S99, 34E10, 34B09.

Keywords. Thin plates · Asymptotics · Wrinkling · Energy methods.

1. Introduction

Approximation schemes such as the Rayleigh-Ritz method or the Galerkin technique have played a historical role in the development of the theory of elastic stability [1,2]. They are still used on a large scale in the engineering community and feature most prominently as the basis of sophisticated finite element computer packages. The use of the more basic "incarnations" of these two methods (in the spirit of Timoshenko's book, for example) represents one of the most expedient ways for solving buckling problems with a relatively modest amount of effort. Unfortunately, these more basic versions are not well suited for describing localised eigendeformations unless one is prepared to allow for a large number of terms in the corresponding approximations. It is precisely such localised effects that we have in mind, and one of our main aims here is to propose a simple, yet efficient, modified energy strategy that circumvents these shortcomings. We start with a brief detour that motivates the work in the subsequent sections.

By considering inhomogeneously stressed rectangular and annular elastic plates subjected to some form of uniform in-plane stretching (see Figs. 1, 6 later in the paper for details of the precise setting), the corresponding linear bifurcation equations for those configurations were found to be intimately controlled by a typically large dimensionless parameter $\mu \gg 1$ (whose definition was problem-dependent). Regular/periodic features of the eigendeformation in one of the two principal directions of the pre-buckling state of stress facilitated the reduction of the corresponding PDEs to ODEs for an unknown transverse amplitude function W. With the help of singular perturbation methods, the critical load λ and the eigenfunction W were then represented as power series in $\mu^{-1/2}$, that is

$$\begin{Bmatrix} \lambda \\ W \end{Bmatrix} = \sum_{j=0}^{\infty} \begin{Bmatrix} \lambda_j \\ W_j \end{Bmatrix} \mu^{-j/2}, \tag{1}$$

with the coefficients $\lambda_j \in \mathbb{R}$ and the functions W_j determined sequentially. An indication of the role played by the size of μ on the accuracy of the approximations derived in [3–6] is included in Tables 1 and 2.

Table 1. *Typical comparisons for the critical edge-buckling loads λ_C of the clamped rectangular plate studied in* [3,4]. Direct numerical simulations (NUM), two-term asymptotic results (ASY I), and three-term asymptotic expressions (ASY II); the relative errors (R.E.) of the last two sets of data with respect to the first are recorded in the last two columns

μ	NUM	ASY (I)	ASY (II)	R.E. I (%)	R.E. II (%)
400.0	0.213362	0.205769	0.212336	3.5588	0.4809
200.0	0.238152	0.221965	0.235099	6.7969	1.2819
80.0	0.300362	0.254101	0.286936	15.4015	4.4697
60.0	0.333067	0.267628	0.311407	19.6475	6.5030
40.0	0.399122	0.290318	0.355988	27.2608	10.8073
10.0	1.226536	0.413969	0.676648	66.2489	44.8326

Table 2. *Same data as in Table 1, but for the annular plate discussed in* [5,6] *(with the corrected term λ_2^* as given in our Sect. 4). Here the ratio of the two radii of the annulus (η) is equal to* 0.1

μ	NUM	ASY (I)	ASY (II)	R.E. I (%)	R.E. II (%)
1200.0	0.197795	0.177290	0.195899	10.3668	0.9583
800.0	0.229288	0.197506	0.225421	13.8611	1.6867
400.0	0.311650	0.243140	0.298969	21.9830	4.0691
200.0	0.454089	0.307676	0.419334	32.2432	7.6538
80.0	0.854713	0.435724	0.714869	49.0210	16.3616
60.0	1.081105	0.489620	0.861813	54.7111	20.2841
40.0	1.556522	0.580031	1.138320	62.7354	26.8677
10.0	7.743505	1.072726	3.305881	86.1468	57.3077

It must be clear from these data that the asymptotic formulae perform admirably well for the range they were intended to, but as μ decreases their reliability deteriorates fast. This trend is more pronounced in the case of the annular plate, so the question arises: can those results be improved?

As pointed out in [5], typical values of the non-dimensional parameter μ for annular thin films are in the vicinity of 300.0 or larger, but smaller numbers are also relevant to practical applications. Thus, extending the results in the aforementioned works to a broader range of values for the stiffness parameter μ would be desirable. Furthermore, from a strictly mathematical point of view, the limit $\mu \to 0$ is also of interest, and this is relevant to the classical case of buckling for an unstretched plate under in-plane bending moments.

The route we choose to pursue the answer to the question posed above is related to the so-called *Hybrid Galerkin Method* discussed at length by Geer and Andersen in a number of interesting papers [7–9][1]. The essence of their method is simple, but it usually requires two distinct steps. In the first stage, perturbation methods are used to produce an expansion similar to (1); this is expected to work well when $\mu \gg 1$ and can be obtained by either regular or singular perturbation techniques, depending on the particular details of the problem at hand. The second stage dispenses with that assumption by replacing the various powers of μ with arbitrary-independent variables that are subsequently found in exactly the same way as in the classical versions of the Rayleigh-Ritz or Galerkin methods.

Gristchack et al. [10] have used the classical WKB method in conjunction with the theory developed in [7–9] to determine the state of stress in an orthotropic elastic conical shell subjected to axial loading, while in [11] they dealt with the problem of dynamic loading for a piezoelectric sandwich plate. Whiting [12] modified existing multiple-scale results for buckling of a long strut on a nonlinear Winkler foundation and used them as a starting point for his Galerkin procedure. That study was later extended by Wadee et al. [13] for the stability of single-hump localised solutions in the same particular context.

[1]The idea of using boundary-layer type functions in conjunction with Galerkin methods can be traced back to much earlier studies like that of Di Prima [16], for example.

The very good accuracy obtained in all of these works is indicative of the high efficiency and reliability of the hybrid approximation methods.

The paper is organised as follows. We start by setting the stage in the next section, where the main ingredients of the energy method for elastic plates are briefly recalled. In Sect. 3, we discuss the details of the modification we introduce for the case of the rectangular plate studied in [3,4]. It is shown that the results obtained with the current strategy do improve the previous studies, especially for the range $\mu \simeq 20.0 \div 300.0$, but difficulties are still encountered for $\mu \lesssim 7.0 \div 10.0$. Partly motivated by this occurrence, we discuss the regular perturbation case $\mu \to 0$ and establish that the relative errors of the new approximations are within 5 % for $0 < \mu \lesssim 2.0$; while the work in Sect. 3.2 is pursued from a purely mathematical perspective, it is particularly gratifying that its range of validity extends well beyond its theoretical limitations. The more difficult problem of the stretched annular plate investigated in [5,6] is tackled in Sect. 4 by using the same modified energy method. Again, comparisons with the earlier results and direct numerical simulations of the original equation show a marked improvement. We conclude with a discussion of the main findings, together with suggestions for further study.

2. Classical energy methods

The energy method is described at length in any good text on elastic stability [1,2,14,15], to which the reader is referred for detailed accounts. Included below is just a sketch of the main ideas and the significant facts relevant to the rest of the paper.

We consider a thin elastic plate whose mid-surface is mathematically represented by a two-dimensional domain $\Omega \subset \mathbb{R}^2$; attached to this plane, there is an arbitrary system of coordinates whose z axis is perpendicular to it, so that the mid-surface can be described by the equation $z = 0$. If $\lambda > 0$ represents the generic loading parameter, the total energy of the plate, E_λ (say), is assumed to split up additively into two contributions: the bending energy, E_{bend}, and the stretching energy, E_{stretch}, that is $E_\lambda(\boldsymbol{u}) = E_{\text{bend}}(\boldsymbol{u}) + E_{\text{stretch}}(\boldsymbol{u})$, where $\boldsymbol{u}$ is the displacement field characterising the deformation of the plate mid-surface. The Kirchhoff-Love assumption in classical plate theory is based on a special approximation of the Lagrangian deformation tensor,

$$\boldsymbol{L} = \frac{1}{2}\left(\boldsymbol{\nabla} \otimes \boldsymbol{v} + \boldsymbol{v} \otimes \boldsymbol{\nabla}\right) - z\boldsymbol{\nabla} \otimes \boldsymbol{\nabla} w + \frac{1}{2}\left(\boldsymbol{\nabla} w\right) \otimes \left(\boldsymbol{\nabla} w\right),$$

where the three-dimensional displacement field is assumed to admit the decomposition $\boldsymbol{u} = \boldsymbol{v} + w\boldsymbol{n}$, with $\boldsymbol{v} = (v^\alpha)_{\alpha=1,2}$ the in-plane part and w the out-of-plane contribution; here $\boldsymbol{n}$ is the unit normal to the oriented mid-surface of the plate.

The inextensional plate theory that lies at the foundation of our analysis is built on the assumption that there is no stretching in the plate midplane, that is $\boldsymbol{L}\big|_{z=0} \simeq \boldsymbol{0}$ or, more explicitly,

$$(\boldsymbol{\nabla} \otimes \boldsymbol{v})^s \simeq -\frac{1}{2}(\boldsymbol{\nabla} w) \otimes (\boldsymbol{\nabla} w), \tag{2}$$

with $(\boldsymbol{\nabla} \otimes \boldsymbol{v})^s$ being the symmetric part of the gradient of the in-plane displacement field $\boldsymbol{v}$. Letting $D > 0$ be the bending rigidity of the plate, the individual energy contributions referred to above can be expressed as

$$E_{\text{bend}}(\boldsymbol{u}) := \frac{1}{2} D \int\limits_{\Omega} \left\{ (\nabla^2 w)^2 - (1-\nu)[w,w] \right\} \mathrm{d}A \tag{3}$$

and

$$
\begin{aligned}
E_{\text{stretch}}(\boldsymbol{u}) := \int_\Omega \boldsymbol{N} : (\boldsymbol{\nabla} \otimes \boldsymbol{v})^s \, \mathrm{d}A &\equiv \int_\Omega (\boldsymbol{\nabla} \otimes \boldsymbol{v})^s : \mathbb{C} : (\boldsymbol{\nabla} \otimes \boldsymbol{v})^s \, \mathrm{d}A \\
&\simeq \frac{1}{4} \int_\Omega (\boldsymbol{\nabla} w) \otimes (\boldsymbol{\nabla} w) : \mathbb{C} : (\boldsymbol{\nabla} w) \otimes (\boldsymbol{\nabla} w) \, \mathrm{d}A \\
&\simeq -\frac{1}{2} \int_\Omega (\boldsymbol{\nabla} \otimes \boldsymbol{v})^s : \mathbb{C} : (\boldsymbol{\nabla} w) \otimes (\boldsymbol{\nabla} w) \, \mathrm{d}A, \qquad (4)
\end{aligned}
$$

where use has been made of Eq. (2). Here, the notation $[f, g] := (\nabla^2 f)(\nabla^2 g) - (\boldsymbol{\nabla} \otimes \boldsymbol{\nabla} f) : (\boldsymbol{\nabla} \otimes \boldsymbol{\nabla} g)$ stands for the Monge-Ampère bracket, '$\otimes$' is the usual tensor product, and the colon "$:$"denotes the double contraction between tensors. The *linearised* membrane stress tensor $\boldsymbol{N} = (N^{\alpha\beta})$ is related to the linearised Lagrangian strain tensor $(\boldsymbol{\nabla} \otimes \boldsymbol{v})^s$ with the help of the usual fourth-order membrane stiffness tensor $\mathbb{C} = (C^{\alpha\beta\gamma\delta})$ through the relation $\boldsymbol{N} = \mathbb{C} : (\boldsymbol{\nabla} \otimes \boldsymbol{v})^s$. For the sake of completeness, we record below the expression of its components,

$$
C^{\alpha\beta\gamma\delta} = \frac{Eh}{2(1+\nu)} \left[\frac{2\nu}{1-\nu} g^{\alpha\beta} g^{\gamma\delta} + g^{\alpha\gamma} g^{\beta\delta} + g^{\alpha\delta} g^{\beta\gamma} \right],
$$

where $(g^{\alpha\beta})$ are the contravariant components of the two-dimensional identity tensor $\boldsymbol{I}, E$ is Young's modulus and ν represents Poisson's ratio.

If we agree to denote by "$\circ$" all pre-bifurcation fields, the flat basic state ($\mathring{w} \equiv 0$) is determined by the vanishing of the first variation of E_λ at $\boldsymbol{u} = \mathring{\boldsymbol{u}}$,

$$
\delta E_\lambda(\mathring{\boldsymbol{u}})[\boldsymbol{h}] \equiv -2 \int_\Omega (\boldsymbol{\nabla} \cdot \mathring{\boldsymbol{N}}) \cdot (\delta \boldsymbol{v}) \, \mathrm{d}A = 0,
$$

for all virtual displacement fields $\boldsymbol{h} = \delta \boldsymbol{v} + 0\boldsymbol{n}$ compatible with the geometrical boundary conditions. The determination of the neutrally stable buckling configurations is then obtained from the well-known Trefftz criterion,

$$
\delta^2 E_\lambda(\mathring{\boldsymbol{u}})[\boldsymbol{u}_C, \boldsymbol{h}] = 0, \qquad (5)
$$

that must be satisfied by all $\boldsymbol{h} = \delta \boldsymbol{v} + (\delta w)\boldsymbol{n}$ compatible with the geometrical boundary conditions; this variational problem defines the critical eigenvalue, $\lambda = \lambda_C$ and the infinitesimal buckling mode $\boldsymbol{u} = \boldsymbol{u}_C$. We recall that the second variation is the bilinear functional defined by

$$
\begin{aligned}
\delta^2 E_\lambda(\mathring{\boldsymbol{u}})[\boldsymbol{h}_1, \boldsymbol{h}_2] := D \int_\Omega & \nabla^2(\delta w_1) \nabla^2(\delta w_2) - (1-\nu)[\delta w_1, \delta w_2] \, \mathrm{d}A \\
& - \int_\Omega \mathring{\boldsymbol{N}} : \boldsymbol{\nabla}(\delta w_1) \otimes \boldsymbol{\nabla}(\delta w_2) \, \mathrm{d}A, \qquad (6)
\end{aligned}
$$

where the virtual displacements $\boldsymbol{h}_j \equiv \delta \boldsymbol{v}_j + (\delta w_j)\boldsymbol{n}$ $(j = 1, 2)$ are assumed to comply with the geometric boundary conditions. The Eq. (5) forms the basis of the classical Rayleigh-Ritz method. By expanding the unknown transverse eigendisplacement in the form $w \simeq w_k := \sum_{j=1}^{k} C_j \phi_j$, where $C_j \in \mathbb{R}$ $(j = 1, 2, \ldots, k)$ are undetermined constants, and the functions $\{\phi_j\}$ are a priori known and assumed to satisfy the kinematic boundary conditions for the problem at hand, the Trefftz criterion translates into the criticality conditions $\partial(\delta^2 E)/\partial C_i = 0$ for $i = 1, 2, \ldots, k$. This typically represents a matrix eigenvalue problem that can be solved easily.

The strategy we propose in this work differs in several respects from the classical method. For example, to allow convergence in the $L^2(\Omega)$-norm of the sequence of approximations, one would have to require that the shape functions $\{\phi_i\}$ form a complete set in Ω; the agreement with the actual solution usually improves by increasing $k \in \mathbb{N}$. Our choice of basis functions does not fulfil such requirements as it is informed by the asymptotic analysis developed in [4,6]. Also, the kinematic boundary conditions are satisfied only approximately, unlike in the classical case. More specific features of our approach will be pointed out as we go along.

3. Rectangular plate

A detailed numerical and asymptotic analysis for the edge-buckling of a stretched elastic plate subjected to in-plane bending was carried out in [3,4]. For the sake of completeness here, we include an outline of the model and a summary of some of the main results.

The rectangular thin elastic plate of length $2a$, width b, and thickness h ($h/b \ll 1$) corresponds to the situation illustrated in Fig. 1; it is assumed to occupy the domain $\Omega \equiv \{(x,y) \in \mathbb{R}^2 \mid -a \le x \le a, 0 \le y \le b\}$.

The plate is stretched by normal stresses σ_0 in the y-direction, while on the two lateral edges, it is subjected to the loads P at the midpoints. Further in-plane bending moments M act simultaneously, as indicated in the aforementioned figure. Under the combined action of these loads, the plate develops a region of compressive stresses adjacent to one of the long edges, leading eventually to a regular wrinkling pattern in the $x-$direction (for a certain critical value of the ratio M/P). With the short sides taken as simply supported, the linearised Donnell-von Kármán buckling equation used for describing the bifurcations of this plate is reduced to an ODE by expressing the transverse displacement in the form $w(x,y) = W(y)\sin(A_m x)$. Eventually, it transpires that

$$W''''(y) + \mathcal{P}_1(\mu, A_m)W''(y) + \mathcal{P}_2(y;\mu, A_m)W(y) = 0, \qquad 0 < y < 1, \tag{7}$$

where

$$\mathcal{P}_1(\mu, A_m) := -(\mu^2 + 2A_m^2),$$
$$\mathcal{P}_2(y;\mu, A_m) := A_m^2 \left\{ A_m^2 + 6\mu^2 \left[2\lambda y - \left(\lambda - \frac{1}{6} \right) \right] \right\},$$

and

$$\eta := \frac{a}{b}, \quad A_m := \frac{m\pi}{\eta}, \quad \lambda := \frac{M}{Pb}, \quad \mu^2 := 12(1-\nu^2)\left(\frac{\sigma_0}{E}\right)\left(\frac{b}{h}\right)^2.$$

The mode number $m \in \mathbb{N}$ is uniquely determined by identifying the global minimum of the curve $\lambda = \lambda(A_m)$. We shall use the appellative 'critical' in relation to these values.

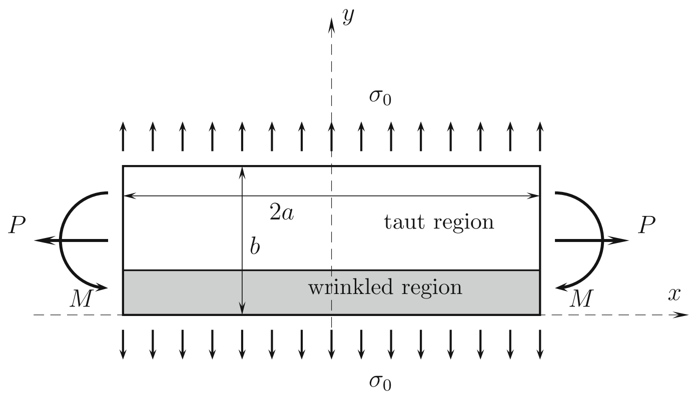

Fig. 1. Stretched thin film under in-plane bending

The same normal-mode solution transforms the boundary conditions along the long edges into relatively simple expressions. In the case of clamped edges, they take the form

$$W = W' = 0 \qquad \text{at} \qquad y = 0, 1, \tag{8}$$

while for the free-edge case, we have

$$W'' - \nu A_m^2 W = 0 \qquad \text{at} \qquad y = 0, 1, \tag{9a}$$

$$W''' - \left[\mu^2 + (2-\nu)A_m^2\right] W = 0 \qquad \text{at} \qquad y = 0, 1. \tag{9b}$$

Finally, the work in [4] provides the asymptotic expansion for the critical buckling load λ_C and the corresponding critical buckling mode number (proportional to A_m^C below) in the form

$$W = W_0(Y) + \mu^{-1/2}W_1(Y) + \mu^{-1}W_2(Y) + \mu^{-3/2}W_3(Y) + \mathcal{O}(\mu^{-2}), \qquad Y := \mu^{1/2}y, \tag{10a}$$

$$\lambda_C = \lambda_0 + \lambda_{1i}^*\mu^{-1/2} + \lambda_{2i}^*\mu^{-1} + \mathcal{O}(\mu^{-3/2}), \quad \text{for} \quad i = 1,\, 2, \tag{10b}$$

$$(A_m^C)^2 = M_{0i}^*\mu^{3/2} + M_{1i}^*\mu + \mathcal{O}(\mu^{1/2}), \quad \text{for} \quad i = 1,\, 2, \tag{10c}$$

where the extra subscript '1' is used to indicate the values for the free-edge case, and '2' applies to the clamped-edge approximation. The coefficients that appear in (10) are recorded below and are identified through a sequence of lengthy matched asymptotic calculations,

$$\begin{aligned}
&\lambda_0 = 1/6, \qquad && M_{02}^* = 1.17306, \qquad && M_{01}^* = 0.62912,\\
&\lambda_{12}^* = 0.78204, \qquad && \lambda_{22}^* = 2.62679, \qquad && M_{12}^* = 0.79737,\\
&\lambda_{11}^* = 0.41941, \qquad && \lambda_{21}^* = 0.65966 - 0.11111\nu^2, \qquad && M_{11}^* = 0.39579 - 0.66666\nu^2.
\end{aligned}$$

Details on the W_j−terms in the expansion of the eigenfunctions are given in the next section (as adapted to our immediate purposes). The comparison between these asymptotic results and numerics showed good agreement for both the two- and three-term approximations when $\mu \gg 1$; the question here is whether or not this assumption can be relaxed without affecting the accuracy.

3.1. Modified energy method

We start by noticing that setting $\boldsymbol{h} \to \boldsymbol{u}_C$ in (5) gives

$$\delta^2 E_\lambda(\mathring{\boldsymbol{u}})[\boldsymbol{u}_C, \boldsymbol{u}_C] = 0\,; \tag{11}$$

in the case of our rectangular plate this equation assumes the form

$$\int_0^1 \Big[W''^2(y) + (\mu^2 + 2A_m^2)W'^2(y) + \mathcal{P}_2(y; \mu, A_m)W^2(y)\Big]\,\mathrm{d}y = 0. \tag{12}$$

Alternatively, the energy integral (12) can be also obtained by multiplying equation (7) by $W \equiv W(y)$ and then integrating the resulting expression over $[0, 1]$ with the help of the corresponding boundary conditions and the integration by parts formula.

As already pointed out, since our main interest lies with the approximation of the envelope of the neutral stability curves, we are essentially looking for eigenvalues satisfying $\partial\lambda/\partial A_m = 0$. On differentiating (12) with respect to A_m^2 and making use of the boundary conditions (8), we derive an extra integral constraint applicable to the case in which the long edges are clamped,

$$\int_0^1 \bigg\{W'^2(y) + \Big[A_m^2 + 3\mu^2\Big(2\lambda y - \Big(\lambda - \frac{1}{6}\Big)\Big)\Big]W^2(y)\bigg\}\mathrm{d}y = 0. \tag{13}$$

An alternative route for arriving at Eq. (13) was given by one of us in [4], and it relies on the use of the Fredholm solvability condition for a certain inhomogeneous fourth-order ODE.

The counterpart of (13) for the case when the long edges of the plate are 'free' rather than 'clamped' is obtained similarly, with the only difference that this time we need to make use of the boundary conditions (9). The final result reads

$$\int_0^1 \left\{ -\nu W(y)W''(y) + (1-\nu)W'^2(y) + \left[A_m^2 + 3\mu^2\Big(2\lambda y - \Big(\lambda - \frac{1}{6}\Big)\Big)\right] W^2(y)\right\} \mathrm{d}y = 0. \tag{14}$$

A possible candidate for the ansatz of our modified energy method is

$$\lambda_C = \lambda_0 + \lambda_{1j}^* c_1, \quad (A_m^C)^2 = M_{0j}^* c_2, \tag{15a}$$

$$W(y) = W_0(y) + W_1(y)c_3 + \cdots, \tag{15b}$$

where

$$W_0(y) = \mathrm{Ai}\Big(\omega\mu^{1/2}y + \zeta_{0j}\Big), \qquad \omega := (2M_{0j}^*)^{1/3}, \tag{16}$$

is $W_0(Y)$ in (10a) expressed in terms of y, and ζ_{0j} denotes the first zero of the equation $Ai^{(j)}(\zeta) = 0$ $(j = 1, 2)$; for the free-edge case, we take $\zeta_{01} \simeq -1.01879$, while for clamped edges, $\zeta_{02} \simeq -2.3381$. The expression of $W_1(y)$ (which is just $W_1(Y)$ in (10a) expressed in terms of y) is not given here because of its high complexity, but it can be found in [4] (see Eqs. 16 and 17) in that reference).

The above approximation is obtained from (10) in which the powers of μ have been replaced by the arbitrary constants c_i $(i = 1, \ldots, n)$; for notational simplicity, we let $\mathbf{c} := [c_1, c_2, \ldots, c_n]$. Note that (15a) do not require more terms as in (10b) or (10c)—it is just the expansion (15b) that could potentially improve the accuracy of our numerical strategy.

If we confine ourselves to the case when just $W_0(y)$ is used in (15b), we essentially end up with two unknowns for which we need only two equations. Substituting (15) into the integral constraint (12) yields a first nonlinear equation in the c_i's, which we shall identify by the notation $f_1(\boldsymbol{c}) = 0$. A second equation is obtained by plugging the same ansatz into either (13) or (14); this will generically be referred to as $f_2(\mathbf{c}) = 0$. Thus, we get two nonlinear equations in two unknowns. Below we provide some details together with a number of simplifications for the concrete case of clamped edges that is investigated numerically at the end of this section (similar calculations can be easily worked out for other type of boundary constraints).

To begin with, we rewrite the energy integral in (12) in the form

$$\int_0^1 \Big[W''^2(y) - \mathcal{P}_1(\mu; A_m)W'^2(y) + \mathcal{R}_1(\mu; A_m, \lambda)W^2(y) + \mathcal{R}_2(\mu; A_m, \lambda)yW^2(y)\Big]\, \mathrm{d}y = 0, \tag{17}$$

where

$$\mathcal{R}_1(\mu; A_m, \lambda) := A_m^2 \left[A_m^2 - 6\mu^2 \left(\lambda - \frac{1}{6}\right)\right],$$

$$\mathcal{R}_2(\mu; A_m, \lambda) := 12\mu^2 A_m^2 \lambda.$$

As mentioned earlier, we choose an ansatz based on the leading-order asymptotic prediction $W(y) = \mathrm{Ai}(ky + \zeta_{02})$, where Ai is the usual Airy function of the first kind, $k := \mu^{1/2}\omega = \mu^{1/2}(2M_{02}^*)^{1/3}$, and M_{02}^* is a constant that has already been mentioned in Sect. 3. To simplify the notation, we then introduce the new variable $Z := ky+\zeta_{02}$, so that now $W(y) = \mathrm{Ai}(Z)$. Furthermore, notice that $d^n(\cdot)/dy^n = k^n d^n(\cdot)/dZ^n$ together with

$$Z\big|_{y=0} = \zeta_{02} =: a_1 \quad \text{and} \quad Z\big|_{y=1} = k + \zeta_0 =: a_2\,;$$

the temporary re-labelling of the first zero of the Airy function is done in order to provide a more uniform notation in the subsequent calculations.

By using the change of variable just introduced above, the integrals in (17) can be recast as following

$$\int_0^1 \left[\frac{\mathrm{d}^2 W}{\mathrm{d}y^2}(y)\right]^2 \mathrm{d}y = k^3 \int_{a_1}^{a_2} Z^2 W^2(Z)\,\mathrm{d}Z,$$

$$\int_0^1 \left[\frac{\mathrm{d}W}{\mathrm{d}y}(y)\right]^2 \mathrm{d}y = k \int_{a_1}^{a_2} \left[\frac{\mathrm{d}W}{\mathrm{d}Z}(Z)\right]^2 \mathrm{d}Z,$$

$$\int_0^1 W^2(y)\mathrm{d}y = \frac{1}{k}\int_{a_1}^{a_2} W^2(Z)\,\mathrm{d}Z,$$

$$\int_0^1 yW^2(y)\mathrm{d}y = \frac{1}{k^2}\int_{a_1}^{a_2} ZW^2(Z)\,\mathrm{d}Z - \frac{a_1}{k^2}\int_{a_1}^{a_2} W^2(Z)\mathrm{d}Z.$$

Therefore, (17) can be further re-arranged as

$$k^3 T_1 - k\mathcal{P}_1(\mu; A_m)T_2 + \left[\frac{\mathcal{R}_1(\mu; A_m,\lambda)}{k} - \frac{a_1\mathcal{R}_2(\mu; A_m,\lambda)}{k^2}\right] T_3 + \frac{\mathcal{R}_2(\mu; A_m,\lambda)}{k^2} T_4 = 0, \tag{18}$$

where

$$T_1 := \int_{a_1}^{a_2} \left[\frac{\mathrm{d}^2 W}{\mathrm{d}Z^2}(Z)\right]^2 \mathrm{d}Z, \qquad T_2 := \int_{a_1}^{a_2} \left[\frac{\mathrm{d}W}{\mathrm{d}Z}(Z)\right]^2 \mathrm{d}Z,$$

$$T_3 := \int_{a_1}^{a_2} W^2(Z)\mathrm{d}Z, \qquad T_4 := \int_{a_1}^{a_2} ZW^2(Z)\mathrm{d}Z.$$

Reference [17] provides us with a set of interesting formulae that facilitate the simplification of integrals of products of Airy functions. That strategy will be applied in the context of (18) as indicated below,

$$T_1 := \int_{a_1}^{a_2} Z^2\mathrm{Ai}^2(Z)\mathrm{d}Z = \frac{1}{5}\Big[2\Big\{Z\mathrm{Ai}(Z)\mathrm{Ai}'(Z) - \frac{1}{2}\mathrm{Ai}^2(Z)\Big\} - Z^2\mathrm{Ai}'^2(Z) + Z^3\mathrm{Ai}^2(Z)\Big]_{a_1}^{a_2}, \tag{19a}$$

$$T_2 := \int_{a_1}^{a_2} \mathrm{Ai}'^2(Z)\mathrm{d}Z = \frac{1}{3}\left[2\mathrm{Ai}(Z)\mathrm{Ai}'(Z) + Z\mathrm{Ai}'^2(Z) - Z^2\mathrm{Ai}^2(Z)\right]_{a_1}^{a_2}, \tag{19b}$$

$$T_3 := \int_{a_1}^{a_2} \mathrm{Ai}^2(Z)\mathrm{d}Z = \Big[Z\mathrm{Ai}^2(Z) - \mathrm{Ai}'^2(Z)\Big]_{a_1}^{a_2}, \tag{19c}$$

$$T_4 := \int_{a_1}^{a_2} Z\mathrm{Ai}^2(Z)\mathrm{d}Z = \frac{1}{3}\Big[\mathrm{Ai}(Z)\mathrm{Ai}'(Z) - Z\mathrm{Ai}'^2(Z) + Z^2\mathrm{Ai}^2(Z))\Big]_{a_1}^{a_2}, \tag{19d}$$

where $[\psi]_{a_1}^{a_2} \equiv \psi(a_2) - \psi(a_1)$. As mentioned earlier, the integration limits a_1, a_2 depend only on the parameter μ. Thus, with μ given, the quantities $T_i = T_i(\mu)$ (for $i = 1,2,3,4$) can be calculated once and for all. On substituting (19) into (18), we end up with the first equation $f_1(A_m,\lambda) = 0$.

Recall that we have also derived the integral constraint (13), which enforces the criticality condition $\partial\lambda/\partial A_m = 0$. This is re-written in the form

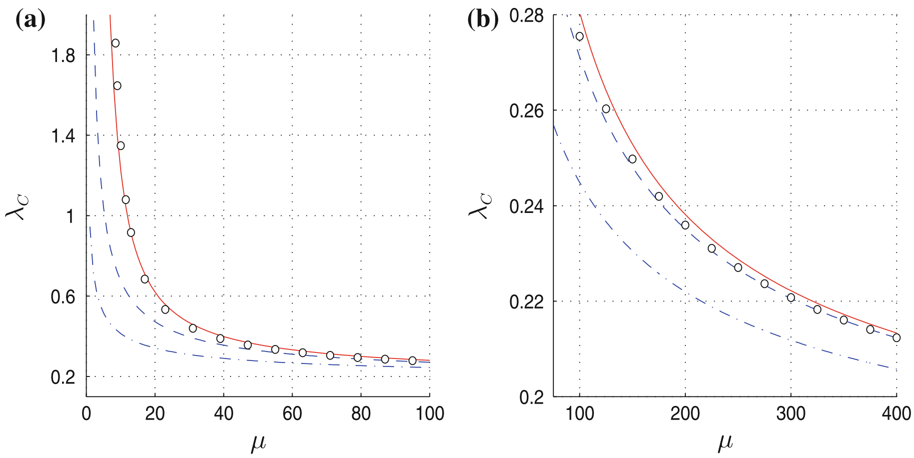

FIG. 2. Comparisons between two- (*dot-dashed line*) and three-term (*dashed line*) asymptotic approximations of the critical eigenvalue, the modified energy method (*small circles*) and the corresponding direct numerical simulations (*continuous line*) for the clamped-edge rectangular plate

$$\int_0^1 \left\{ W'^2(y) + \Big[\mathcal{R}_3(\mu; A_m, \lambda) + \mathcal{R}_4(\mu; A_m, \lambda) y\Big] W^2(y) \right\} \mathrm{d}y = 0, \tag{20}$$

where

$$\mathcal{R}_3(\mu; A_m, \lambda) = A_m^2 - \mu^2 \left(3\lambda - \frac{1}{2}\right), \qquad \mathcal{R}_4(\mu; \lambda) = 6\mu^2\lambda.$$

Carrying out the same transformation on variables as for (17), we eventually get

$$kT_2 + \left[\frac{\mathcal{R}_3(\mu; A_m, \lambda)}{k} - \frac{a_1 \mathcal{R}_4(\mu; \lambda)}{k^2}\right] T_3 + \frac{\mathcal{R}_4(\mu; \lambda)}{k^2} T_4 = 0, \tag{21}$$

where T_2, T_3, T_4 were introduced earlier in (18). If we plug (19) into (21), we then obtain the second equation $f_2(A_m, \lambda) = 0$.

To summarise, we have formulated two nonlinear equations $f_1 = 0, f_2 = 0$ in two unknowns A_m, λ. Since A_m and λ depend only on c_1 and c_2, according to (15), we essentially have two equations in the two unknowns c_1 and c_2. To complete the solution, the multi-dimensional root finding problem is transformed into a minimisation problem by considering $I(\boldsymbol{c}) := f_1^2(\boldsymbol{c}) + f_2^2(\boldsymbol{c})$, which is expected to be zero when $\boldsymbol{c} \in \mathbb{R}^2$ corresponds to our actual solution. Cast in this form the problem is then solved by using Powell's method (e.g., see [18] for details). The situation we are confronted with is not trivial because the functional that needs to be minimised is highly nonlinear. We have checked that the minima of $I(\boldsymbol{c})$ lead to values of the functional that are virtually indistinguishable from zero; this indicates that our approximate solution satisfies the neutral stability condition (12) and guarantees that the most dangerous mode has been captured. A final observation worth stating is that, owing to the non-quadratic nature of the functional to be minimised, providing an initial guess requires additional care. We employed a numerical continuation strategy in which the original guess was supplied by various powers of $\mu \gg 1$, as hinted by (10), with μ then being decreased progressively until it reached $\mathcal{O}(1)-$values.

Results of this method are recorded in Figs. 2 and 3 for clamped and, respectively, free-edge boundary conditions. The direct numerical simulations are shown with a continuous line, while the new approximations are represented by the white markers. To put things in perspective, we have also included the two- and three-term asymptotic approximations from [4] (the dashed/dot-dashed lines). It is quite remarkable that the simple-minded ansatz (16) informed by the leading-order asymptotic analysis of equation (7)

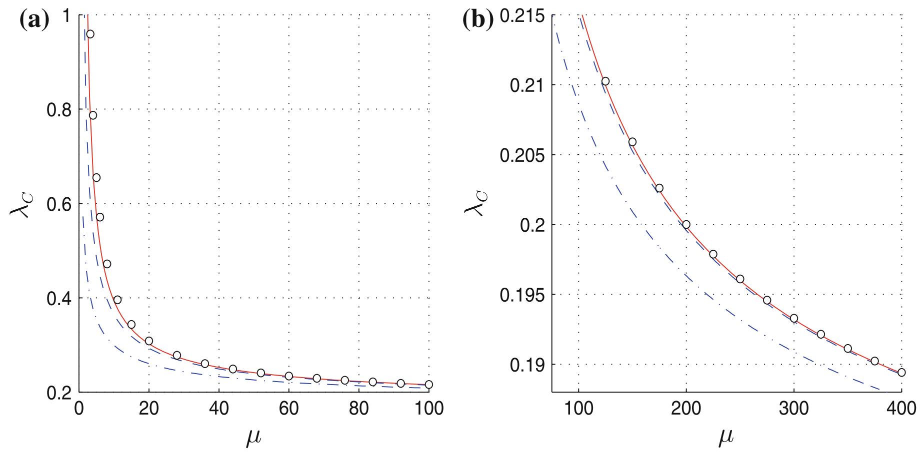

FIG. 3. Same as per Fig. 2, but for the free-edge rectangular plate

outperforms by a long shot the two-term asymptotic approximation obtained through a very laborious analysis [4]. In Fig. 2, the relative errors between the modified energy results and numerics tend to deteriorate for μ below 11.0 (R.E. $\simeq$ 5.14 % in that case), although for $\mu \gtrsim 60.0$ we have R.E. $\lesssim$ 2.73 %. Similar conclusions can be drawn in relation to Fig. 3—see [19] for more details.

A caveat needs to be raised about our choice of test function (16). In the case of a clamped plate, for relatively largish values of μ (typically, greater than 10.0), this function and its derivative display exponential decay for $y \simeq 1.0$, so the constraints $W(1) = W'(1) = 0$ are satisfied asymptotically. Note that by definition $W(0) = 0$ (exactly), but $W'(0) \neq 0$. It was shown in [4] that satisfaction of the latter condition demanded the introduction of an $\mathcal{O}(\mu^{-1})$ layer that had to be matched to the solution described by Eq. (10). Here, we have disregarded this effect because the results obtained with the apparently crude choice of (16) already lead to values that improve considerably upon the earlier studies. In Sect. 5, we shall reconsider this point and look more closely at what happens if the test function is replaced by the $\mathcal{O}(\mu^{-1})$ *composite* asymptotic approximation that partially satisfies the derivative boundary condition at $y = 0$. It is also important to keep in mind that higher-order asymptotic results are not easily available for the annulus problem discussed in Sect. 4.

It might be tempting to try and improve the results already obtained, especially since $W_1(y)$ in (15b) is available [4]. In this case, we have three unknowns, so a change of tack is imperative. The criticality conditions (13) or (14) will remain unchanged, but two further equations are obtained with the help of (5) in which $\delta w \to W_0(y)\sin(A_m x)$ and $\delta w \to W_1(y)\sin(A_m x)$, respectively. Doing this, however, does not lead to any noteworthy headway since the kinematic boundary condition $W'(0) = 0$ is still violated (and will continue to be so as long as we do not take into consideration the $\mathcal{O}(\mu^{-1})$ layer mentioned above).

3.2. The limiting case $\mu \to 0$

As already pointed out in the *Introduction*, for very thin plates, it is the limit $\mu \gg 1$ that matters most. However, from a mathematical point of view, it would be important to understand the asymptotic structure of the opposite limit $\mu \to 0$ as well. This case is relevant to the important situation $\sigma_0 = 0$ and represents an interesting *regular perturbation* problem. We also anticipate that the range of validity for these new asymptotic results will extend beyond their immediate limit of applicability, so they could be useful (at least in principle) as numerical guesses for the optimisation routines used in the modified

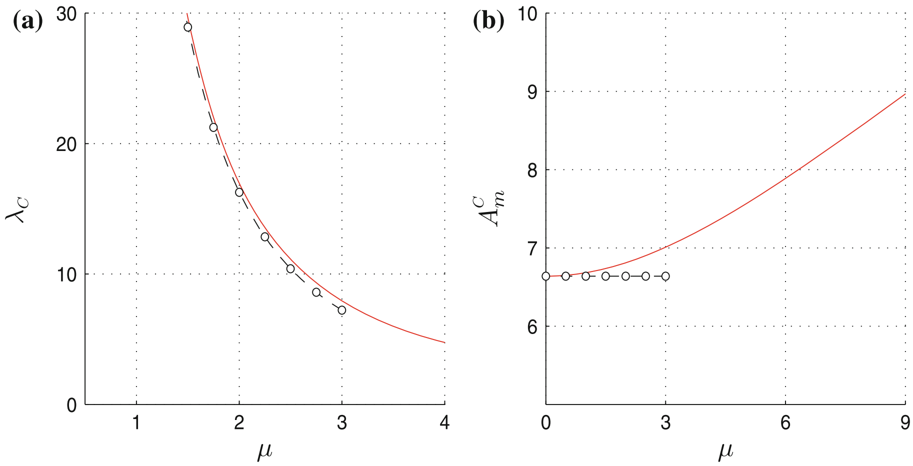

Fig. 4. Comparison between the asymptotic approximation $\lambda_C \simeq \lambda_0^*/\mu^2$ (*circle-dash*) and its counterpart obtained by direct numerical simulations (*continuous line*) in the case of a clamped-edge rectangular plate. The right window gives an idea about a similar comparison involving the corresponding mode numbers

energy method. Another motivation for the work in this section comes from the related papers of Geer and Andersen [7–9], although it will eventually transpire that we cannot follow their strategy very closely.

3.2.1. Clamped-edge boundary conditions. For a rectangular plate with clamped edges $A_m^C = \mathcal{O}(1)$ as $\mu \to 0$. At the same time, the critical eigenvalue λ_C displays a tendency to blow up, which was verified by the direct numerical simulations. This limiting behaviour is captured by the following ansatz

$$W(y) = W_0(y) + W_1(y)\mu^2 + \cdots, \tag{22a}$$

$$\lambda = \lambda_0\mu^{-2} + \lambda_1 + \lambda_2\mu^2 + \cdots, \tag{22b}$$

$$(A_m)^2 = M_0 + M_1\mu^2 + \cdots, \tag{22c}$$

where W_0, λ_0, and M_0 satisfy the simplified differential equation

$$W_0'''' - 2M_0^2 W_0'' + M_0\left[M_0 + 6\lambda_0(2y-1)\right]W_0 = 0, \tag{23}$$

that is to be solved subject to the boundary conditions $W_0 = W_0' = 0$ for $y = 0, 1$. Here, and in the next section, we shall employ some of the labels used previously for expanding λ, A_m and W in order to avoid overdoing the notation; no confusion should arise as these derivations are independent of each other.

Note that this reduced problem depends only on the parameters λ_0 and M_0, so we can integrate it numerically once and for all to identify the values for which the curve $\lambda_0 = \lambda_0(M_0)$ has a global minimum. It is found that the critical values are $(\lambda_0^*, M_0^*) = (65.0663, 6.6399)$.

Some comparisons with direct numerical simulations are included in Fig. 4. It can be clearly seen that the asymptotic solution for $0 < \mu \ll 1$ is applicable even for $0 < \mu \lesssim 2.0$, since its relative error is within 5 % for this range of μ. Unfortunately, the asymptotic analysis can be executed only to the leading order—similar limitations were encountered in a couple of recent works [20,21].

3.2.2. Free edges. For the free-edge case, informed by numerical simulations, we expect the critical A_m to approach zero as $\mu \to 0$ and λ_C is found to display a similar blow-up behaviour as seen previously. However, the asymptotic structure of the limiting case is somewhat different. It turns out that this time we need an ansatz of the form

$$W(y) = W_0(y) + W_1(y)\mu + W_2(y)\mu^2 + \cdots, \tag{24a}$$

$$\lambda = \lambda_0\mu^{-1} + \lambda_1 + \lambda_2\mu + \cdots, \tag{24b}$$

$$(A_m)^2 = M_0\mu^2 + M_1\mu^3 + \cdots. \tag{24c}$$

Substituting (24) into the bifurcation equation (7) and setting to zero the coefficients of successive powers of μ we obtain

$$\mathcal{O}(1): \quad W_0'''' = 0, \tag{25a}$$

$$\mathcal{O}(\mu): \quad W_1'''' = 0, \tag{25b}$$

$$\mathcal{O}(\mu^2): \quad W_2'''' - (1 + 2M_0)W_0'' = 0, \tag{25c}$$

$$\mathcal{O}(\mu^3): \quad W_3'''' - (1 + 2M_0)W_1'' - 2M_1W_0'' + 6M_0(2y - 1)\lambda_0 W_0 = 0. \tag{25d}$$

Similarly, plugging (24) into the boundary conditions (9), we derive the constraints that W_j (for $j = 1, 2, \ldots$) must satisfy at $y = 0, 1$

$$W_0'' = 0, \qquad W_0''' = 0, \tag{26a}$$

$$W_1'' = 0, \qquad W_1''' = 0, \tag{26b}$$

$$W_2'' - \nu M_0 W_0 = 0, \qquad W_2''' - [1 + (2 - \nu)M_0]\, W_0' = 0, \tag{26c}$$

$$W_3'' - \nu M_0 W_1 - \nu M_1 W_0 = 0, \qquad W_3''' - [1 + (2 - \nu)M_0]\, W_1' - (2 - \nu)M_1 W_0' = 0. \tag{26d}$$

Finally, the critical buckling mode condition (14) can be expanded in powers of μ and results in the following additional constraints

$$\mathcal{O}(1): \quad \int_0^1 \left[\nu W_0 W_0'' - (1 - \nu)W_0'^2\right] \mathrm{d}y = 0, \tag{27a}$$

$$\mathcal{O}(\mu): \quad \int_0^1 [\nu W_0 W_1'' - 2(1 - \nu)W_0' W_1' + \nu W_0'' W_1 + \Gamma_1]\, \mathrm{d}y = 0, \tag{27b}$$

$$\mathcal{O}(\mu^2): \quad \int_0^1 [\nu W_0 W_2'' - 2(1 - \nu)W_0' W_2' + \nu W_0'' W_2 + \Gamma_2]\, \mathrm{d}y = 0, \tag{27c}$$

where

$$\Gamma_1 := -3(2y - 1)\lambda_0 W_0^2,$$

$$\Gamma_2 := \nu W_1 W_1'' - (1 - \nu)W_1'^2 - 6(2y - 1)\lambda_0 W_0 W_1 - \left[M_0 + 3(2y - 1)\lambda_1 - \frac{1}{2}\right] W_0^2.$$

The leading order Eq. (25a) together with the boundary conditions (26a) produces the general solution $W_0(y) = \gamma_1 y + \gamma_2$ in which $\gamma_1, \gamma_2 \in \mathbb{R}$ are constants that will be fixed as we go along. On substituting this W_0 into (27a) results in $\gamma_1 = 0$, and hence $W_0(y) = \gamma_2$; without any loss of generality, we can assume $\gamma_2 = 1$.

Next, considering the Eq. (25b) subject to the end constraints (26b) yields $W_1(y) = \gamma_3 y + \gamma_4$, where $\gamma_3, \gamma_4 \in \mathbb{R}$ are constants. Note that γ_4 can be taken to be zero because of the homogeneous nature of the problem and, as we have $W_0(y)$ already, it is only γ_3 that needs to be determined. To this end, we carry on with solving the next order problem, consisting of (25c) in conjunction with (26c); some simple algebra eventually leads to $W_2(y) = \dfrac{1}{2}\nu M_0 \gamma_2 y^2$.

We mention in passing that the criticality constraint (27b) is identically satisfied with the information we have thus far, so we need to look at (27c). It transpires that

$$(1-\nu)\gamma_3^2 + \lambda_0\gamma_2\gamma_3 + \left[(1-\nu^2)M_0 + \frac{1}{2}\right]\gamma_2^2 = 0, \tag{29}$$

an equation that will be used shortly to identify λ_0. After some further manipulations, the solution of (25d) and (26d) is found to be

$$W_3''(y) = -6M_0\left(\frac{y^3}{3} - \frac{y^2}{2}\right)\lambda_0\gamma_2 + \gamma_5 y + \gamma_6, \tag{30}$$

with

$$\gamma_5 := (\nu\gamma_3 - \lambda_0\gamma_2)M_0, \qquad \gamma_6 := \nu M_1\gamma_2\,;$$

in the course of reaching equation (30), it also emerges that

$$\gamma_3 = -\left[\frac{M_0\lambda_0}{1+2(1-\nu)}\right]\gamma_2.$$

On substituting this value of γ_3 into (29), we arrive at

$$\lambda_0^2 = \frac{M_0(1-\nu^2)+\frac{1}{2}}{\omega_2 M_0 - \omega_1 M_0^2}, \tag{31}$$

where

$$\omega_1 := \frac{1-\nu}{[1+2(1-\nu)]^2} \qquad \text{and} \qquad \omega_2 := \frac{1}{1+2(1-\nu)}.$$

As we aim for the lowest critical load, this expression must be minimised with respect to M_0, that is $\partial\lambda_0^2/\partial M_0 = 0$. The result is a quadratic algebraic equation for M_0, whose unique positive root will give the critical value

$$M_0^* = \frac{-1+\sqrt{7+2\nu-4\nu^2}}{2(1-\nu^2)}. \tag{32}$$

The corresponding critical value of λ_0 is obtained by substituting (32) into (31), that is

$$\lambda_0^* = \lambda_0\big|_{M_0=M_0^*}. \tag{33}$$

To assess the relevance and usefulness of these last two formulae, a representative sample of comparisons between them and direct numerical simulations is summarised in Fig. 5.

The remarks made in the previous section vis-á-vis the range of applicability of the results derived for the free-edge case remain valid. Relative errors between asymptotics and numerics are roughly 5 % for $0 < \mu \lesssim 2.0$. Further work, not discussed here, has shown that the term λ_1 in the asymptotic ansatz (24b) is negative. Once obtained, that term does improve the accuracy of the approximation as μ gets closer and closer to zero, but within the range $1.0 < \mu < 2.0$ the results become worse.

4. Annular plate

Full details of this model and a comprehensive asymptotic analysis can be found in [5,6]; only the most important aspects are highlighted below.

We consider an annular plate with inner radius R_1, outer radius R_2, and thickness h ($h \ll R_2$)—as shown in Fig. 6. This configuration is stretched by applying uniform radial displacement fields u_1 and u_2 on the inner and outer rims, respectively. The Lamé solution for the corresponding plane stress problem reveals the presence of compressive stresses near the inner rim. Coupled with the same Donnell-von Kármán buckling equation as in Sect. 3, the bifurcation problem that results is reduced to an ODE by

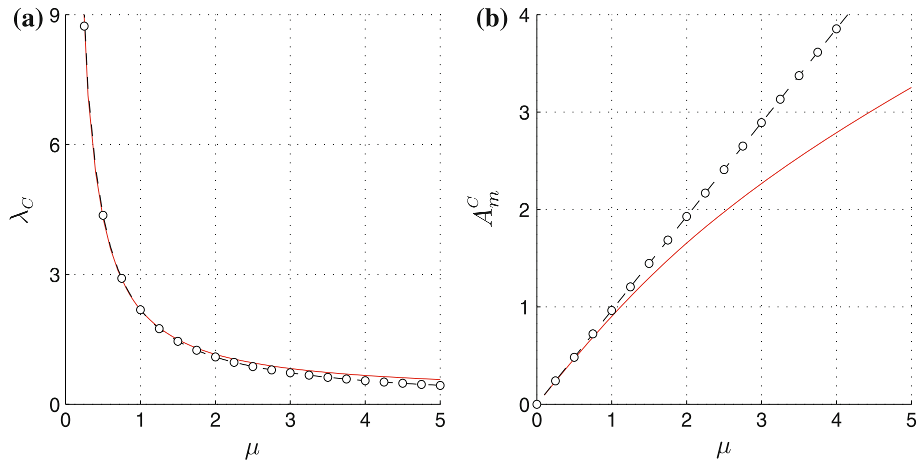

Fig. 5. Free-edge rectangular plate: comparison between the asymptotic approximation $\lambda_C \simeq \lambda_0^*/\mu$ (*small circles*) given by (33) and direct numerical simulations. The accuracy of (24c) and (32) can be appreciated by inspecting the window on the right

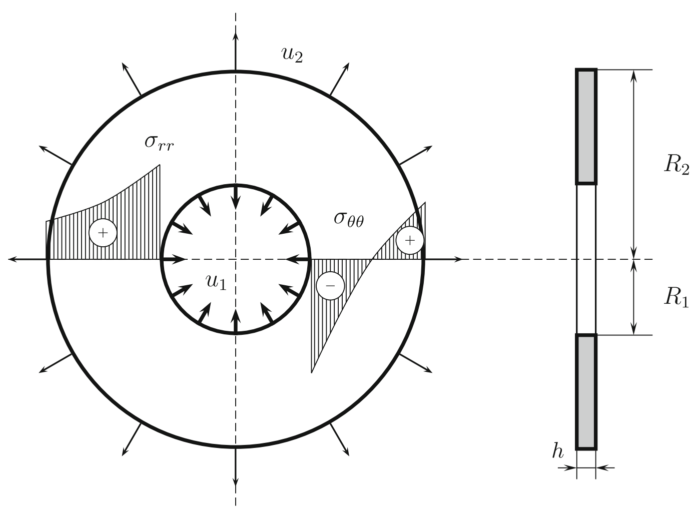

Fig. 6. An annular plate subjected to uniform displacement fields on its boundaries. For a sufficiently large ratio u_1/u_2, localised buckling emerges near the central hole

using the separable variables solution $w(r,\theta) = W(r)\cos n\theta$, where $n \in \mathbb{N}$ is the mode number (equal to half the number of identical wrinkles in the azimuthal direction). The final result reads

$$W'''' + \mathcal{P}_3(\rho)W''' + \mathcal{P}_4(\rho)W'' + \mathcal{P}_5(\rho)W' + \mathcal{P}_6(\rho)W = 0, \quad \eta < \rho < 1, \tag{34}$$

where $\eta := R_1/R_2, \rho := r/R_2$ and the rescaled W is denoted by the same letter to avoid overloading the notation. The coefficients of (34) are defined by

$$\mathcal{P}_3(\rho) := \frac{2}{\rho}, \quad \mathcal{P}_4(\rho) := -\left[\frac{2n^2+1}{\rho^2} + \mu^2\left(A + \frac{B}{\rho^2}\right)\right],$$

$$\mathcal{P}_5(\rho) := \frac{1}{\rho}\left[\frac{2n^2+1}{\rho^2} - \mu^2\left(A - \frac{B}{\rho^2}\right)\right], \quad \mathcal{P}_6(\rho) := \frac{n^2}{\rho^2}\left[\frac{n^2-4}{\rho^2} + \mu^2\left(A - \frac{B}{\rho^2}\right)\right],$$

with

$$A := (1+\nu)\frac{1+\lambda\eta}{1-\eta^2}, \quad B := (1-\nu)\frac{\eta^2+\lambda\eta}{1-\eta^2}, \quad \lambda := \frac{u_1}{u_2}, \quad \mu^2 := \frac{12u_2R_2}{h^2}. \tag{35}$$

For the sake of brevity, only clamped boundary conditions are considered. In terms of the amplitude $W(\rho)$, these are

$$W(\rho) = W'(\rho) = 0 \quad \text{at} \quad \rho = 0, 1. \tag{36}$$

In [6,22], Coman and Bassom provided a detailed asymptotic investigation of the aforementioned model. They showed that the neutral stability envelope can be obtained by various expansions in suitable powers of $\mu \gg 1$,

$$W(Y) = W_0(Y) + W_1(Y)\mu^{-1/2} + \mathcal{O}(\mu^{-1}), \qquad Y := \mu^{1/2}(\rho - \eta), \tag{37a}$$

$$(n_C)^2 = N_0^*\mu^{3/2} + \mathcal{O}(\mu), \tag{37b}$$

$$\lambda_C = \lambda_0 + \lambda_1^*\mu^{-1/2} + \lambda_2^*\mu^{-1} + \mathcal{O}(\mu^{-3/2}), \tag{37c}$$

where

$$N_0^* = \left(\frac{2}{3}\zeta_0\eta^2\hat{A}_0\right)^{3/4}, \quad \lambda_0 = \frac{2\nu\eta}{1-\nu-\eta^2(1+\nu)},$$

$$\lambda_1^* = 4N_0^*G, \qquad \lambda_2^* = 2\eta^2G\left[4\zeta_0(N_0^*)^{2/3}\left(G\widehat{A}_1 + \frac{1}{2\eta^2}\right) + \frac{(\widehat{A}_0)^{1/2}}{\eta\sqrt{2}}\right];$$

$(-\zeta_0) \simeq -2.3381$ represents the first zero of the Airy function Ai, and we have introduced the notations

$$\widehat{A}_0 := \frac{(1+\nu)(1+\lambda_0\eta)}{1-\eta^2}, \quad \widehat{A}_1 := \frac{(1+\nu)\eta}{1-\eta^2}, \quad G := \frac{1-\eta^2}{\eta(1-\nu)-\eta^3(1+\nu)}.$$

Note that in the expansion of $(n_C)^2$, only the critical value N_0^* is available—as pointed out in [6], the effort required to find N_1^* is significant. Thus, improving on these results is far from being a lightweight undertaking.

The modified energy method for the annular plate proceeds along the same route as in Sect. 3.1; the ansatz that we use is given by

$$\lambda \simeq \lambda_C \equiv \lambda_0 + \lambda_1^* c_1, \quad n^2 \simeq (n_C)^2 \equiv N_0^* c_2, \quad W = W_0(Y) + W_1(Y)c_3 + \cdots, \tag{38}$$

where

$$W_0(\rho) = \mathrm{Ai}\left(\frac{N_0^{*1/3}\mu^{1/2}}{\eta}(\rho - \eta) + \zeta_0\right). \tag{39}$$

In this case $W_1(Y)$ is not easily available, so our approximation will have only two degrees of freedom (c_1 and c_2). These constants are found from (11), which for an annular plate becomes

$$\int_\eta^1 \Big[\Pi_3 W''^2(\rho) + \Pi_4 W'^2(\rho) + \Pi_5 W^2(\rho)\Big]\mathrm{d}\rho = 0, \tag{40}$$

with

$$\Pi_3 := \rho, \qquad \Pi_4 := \frac{2n^2+1}{\rho} - \Delta_1(1+\lambda\eta)\rho - \Delta_2\frac{\eta(\lambda+\eta)}{\rho},$$
$$\Pi_5 := \frac{n^2(n^2-4)}{\rho^3} - \frac{n^2}{\rho}\left(\Delta_1 - \frac{\Delta_2}{\rho^2}\right)(\lambda\eta+1),$$

and

$$\Delta_1 := \frac{\mu^2(1+\nu)}{1-\eta^2}, \qquad \Delta_2 := \frac{\mu^2(1-\nu)}{1-\eta^2}.$$

An additional equation is obtained from the criticality condition of $\lambda \equiv \lambda(n)$ with respect to n^2,

$$\int_\eta^1 \Big[\Pi_6 W'^2(\rho) + \Pi_7 W(\rho)W'(\rho) + \Pi_8 W^2(\rho)\Big]\mathrm{d}\rho = 0, \tag{41}$$

where

$$\Pi_6 := \frac{2}{\rho^2}, \quad \Pi_7 := -\frac{2}{\rho^3}, \quad \Pi_8 := \frac{\mu^2}{\rho^2}\left(A - \frac{B}{\rho^2}\right) + \frac{2(n^2-2)}{\rho^4},$$

and the expressions of A and B were defined in (35). These equations will be used in the numerical strategy described in Sect. 3.1 and already employed in the previous section, so we omit the details.

In contrast to the rectangular plate, we now have an extra parameter, $0 < \eta < 1$, so our comparisons between asymptotics and numerics will have to reflect this new addition. Figure 7 shows a first set of comparisons for $\eta = 0.2$ and, respectively, $\eta = 0.4$, similar to the ones included in Figs. 2 and 3. The results of the modified energy method based on the one-term ansatz (39) appear to perform better than both the two- and three-term asymptotic approximations derived in [6]. More specifically, the relative errors between the values computed with the former approach and direct numerical simulations lie between 1.06 and 1.49 % for μ in the range [22.0, 350.0], but they tend to deteriorate quickly as $\mu \simeq 10.0$ because the boundary condition $W(1) = 0$ starts to be violated in that instance. Given our previous experience from Sect. 3.1, this is not unexpected. As shown in [19] that regime can be captured by the low-μ asymptotic analysis, which here is left out in the interest of brevity.

A different set of comparisons is presented in Figs. 8 and 9, which contain the neutral stability envelopes for the stretched annulus. It is known [23] that the individual curves $\lambda = \lambda(\eta; m)$ for $m = 2, 3, \dots$ satisfy $\lim_{\eta\to 0} \lambda(\eta; m) = +\infty$, and therefore the envelope of this family of curves is expected to have the same characteristic. However, the asymptotic analysis proposed in [6] was conducted under the assumption that $\eta = \mathcal{O}_S(1)$, so the approximations of the envelope derived there, and reproduced here as the dash/dash-dot lines for convenience, cannot be expected to be a faithful description of what happens for $\eta \simeq 0$[2]. Interestingly enough, the modified energy approximation is free of such shortcomings, and it appears to follow the numerical envelope quite closely. The relative errors in Fig. 8a are admittedly large because $\mu = 10.0$, but they decrease quickly as this parameter increases. For example, in Fig. 9a ($\mu = 40.0$), they are within 5.20 % for $\eta \in [0.095, 0.5]$, while in Fig. 9d ($\mu = 350.0$), the maximum relative error is 1.5 % for $0.03 < \eta < 0.5$. We also want to point out that the blow-up of λ (both the numerical solution and our current approximations) is present in all four plots in Fig. 9, but it is not emphasised since the $\eta-$region over which this behaviour occurs is awkward to represent graphically; furthermore, this regime has very little relevance from a practical point of view.

[2] This assertion does not contradict the results obtained by Coman and Bassom in [6] since for $\mu \gg 1$ the range of η for which their formula is not accurate is extremely small; in fact, it can be argued that to the level of accuracy of visual inspection, their formulae perform very well for the entire range of *realistic* values of η. As shown in [23] by the first author, (37c) plays the role of some sort of outer approximation for $|\eta - 1| \ll 1$ that can be complemented by a similar expression for $\eta \to 0$.

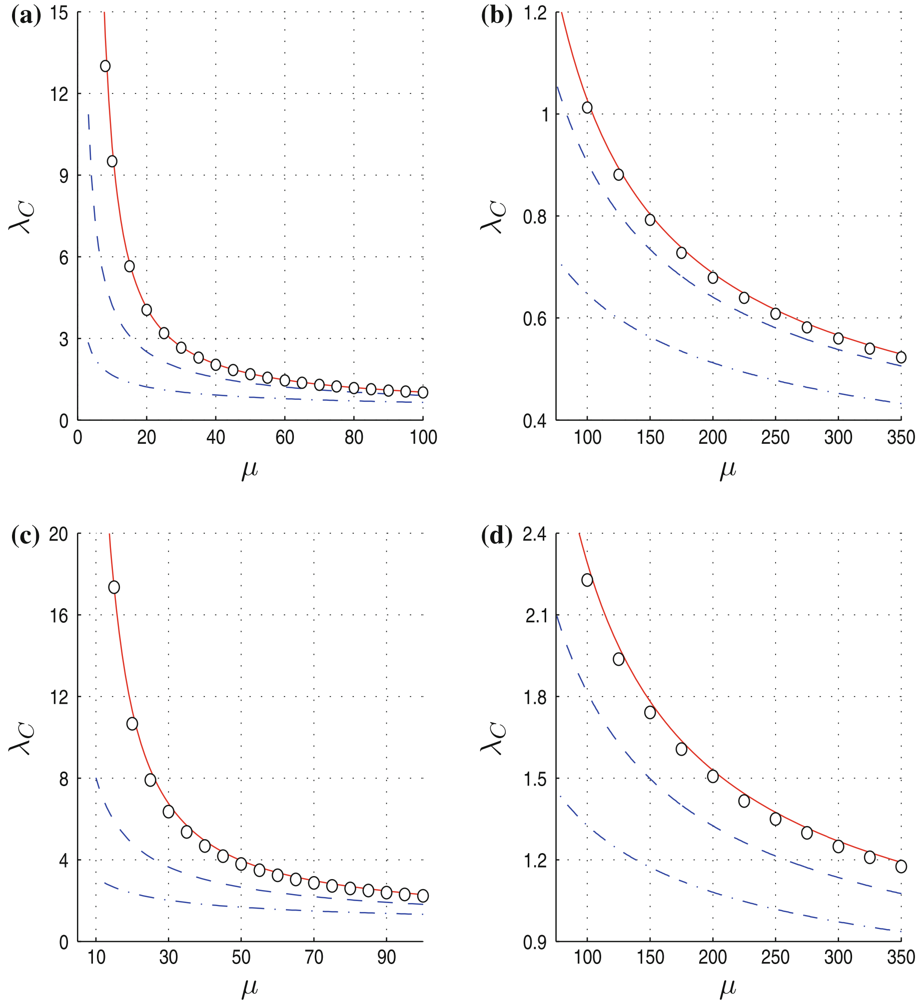

FIG. 7. Comparisons of the various approximations of the critical eigenvalue $\lambda_C \equiv \lambda_C(\mu)$: two- (*dot-dashed line*) & three-term (*dashed line*) asymptotic results, the modified energy method (*small circles*), and the direct numerical results (*continuous line*) for the stretched annular plate. Here $\eta = 0.2$ in (**a**, **b**) and $\eta = 0.4$ in (**c**, **d**)

5. Discussion

Motivated by recent work on the bending instabilities of thin elastic plates in tension (e.g., [4,6]), a modified energy method has been proposed to improve upon those earlier results. With the help of an ansatz informed by the asymptotic structure of the problems at hand, we have showed that the new strategy is capable of producing approximations for both the critical edge-buckling loads and the number of wrinkles that are valid for moderate values of the stiffness parameter μ. It is remarkable that the accuracy achieved is very good despite the simplicity of the ansatz employed. This leads us to believe that leading-order asymptotic approximations in other contexts (such as the two-dimensional problems in [24], for instance) could form the basis for similar energy strategies, thus circumventing the need of complicated numerical work.

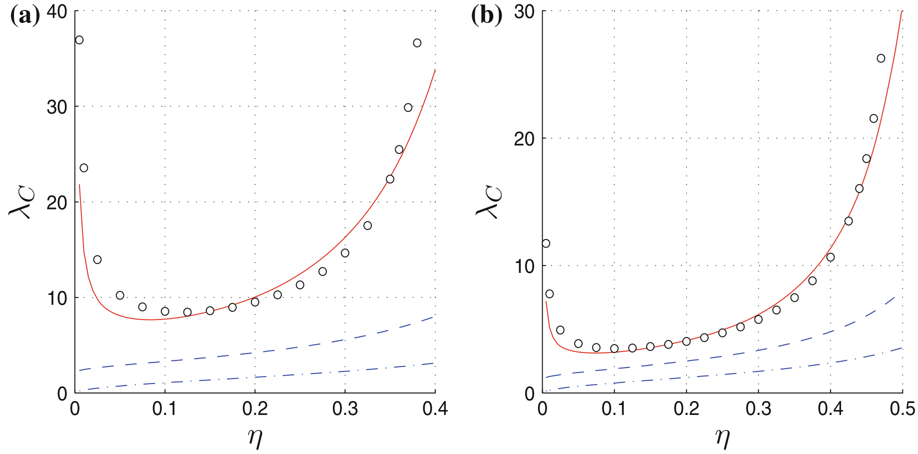

Fig. 8. Dependence on η of the two- (*dot-dashed line*) & three-term (*dashed line*) asymptotic results, the modified energy method (*small circles*), and the direct numerical results (*continuous line*) for the stretched annular plate: $\mu = 10.0$ (**a**) and $\mu = 20.0$ (**b**)

In the context of asymmetric buckling problems, our modified energy method is particularly versatile since it is able to capture the neutral stability envelope with minimum effort. Indeed, this is done by simply adding an extra integral constraint as demanded by the criticality of the eigenvalue with respect to the mode number. It is interesting to note that while the general asymptotic approach in [4] and [6] for rectangular and annular plates, respectively, was identical, its accuracy was problem-dependent. The modified energy method seems to be free of such shortcomings and is quite robust.

It was mentioned in Sect. 3.1 that a more suitable ansatz for the problems discussed in this work would be one that incorporates the effect of the $\mathcal{O}(\mu^{-1})$ bending layer. Prompted by that observation, we shall now consider replacing W in (16) by

$$\widehat{W}(y) = \mathrm{Ai}(Z) + \mu^{-1/2}\big\{\beta_1 \mathrm{Ai}'(Z) + \beta_2 \mathrm{Ai}'''(Z) + \mathrm{Ai}'(\zeta_{02})\exp(-\mu y)\big\}, \tag{42}$$

where $Z := \omega\mu^{1/2}y + \zeta_{02}$ and β_j $(j = 1, 2)$ are the complicated expressions defined in Eq. (17) of [4]. Comparisons with various other results obtained previously are recorded in Table 3. The data included there indicates a significant improvement over both the asymptotic results reported in [6] and our earlier simplified Rayleigh-Ritz strategy. It can be shown that the free-edge case for the rectangular plate is amenable to a similar treatment by following the analysis available in [4], although things are considerably more involved for the annular plate. That is partly due to the fact that one has to take the asymptotic analysis of [6] to the next order ([19] contains the relevant details and some further comparisons).

Refining the ansatz (16) or (39) as indicated above can only provide a sensible improvement as long as μ does not get too small, typically $\mu \gtrsim 10.0$. Indeed, the analysis of Geer and Andersen in [7–9] suggests that for lower μ-values one would have to augment the Rayleigh-Ritz ansatz by terms coming from the asymptotic analysis in which $0 < \mu \ll 1$. Unfortunately, as we have already seen in Sect. 3.2 for the clamped plate, the expression of the corresponding eigenmodes is not immediately available in closed form. While in principle we can construct the refined ansatz and use numerical methods to carry out the programme outlined in Sect. 3.1, there is little scope in pursuing it as this would defeat the whole purpose of using the Rayleigh-Ritz method in the first place.

Finally, the analysis described in this paper reinforces the duality between numerics and asymptotics. By using the techniques of asymptotic analysis, one is naturally led to a correct estimate of the ansatz that needs to be used in approximate methods such as the Rayleigh-Ritz technique. It would be

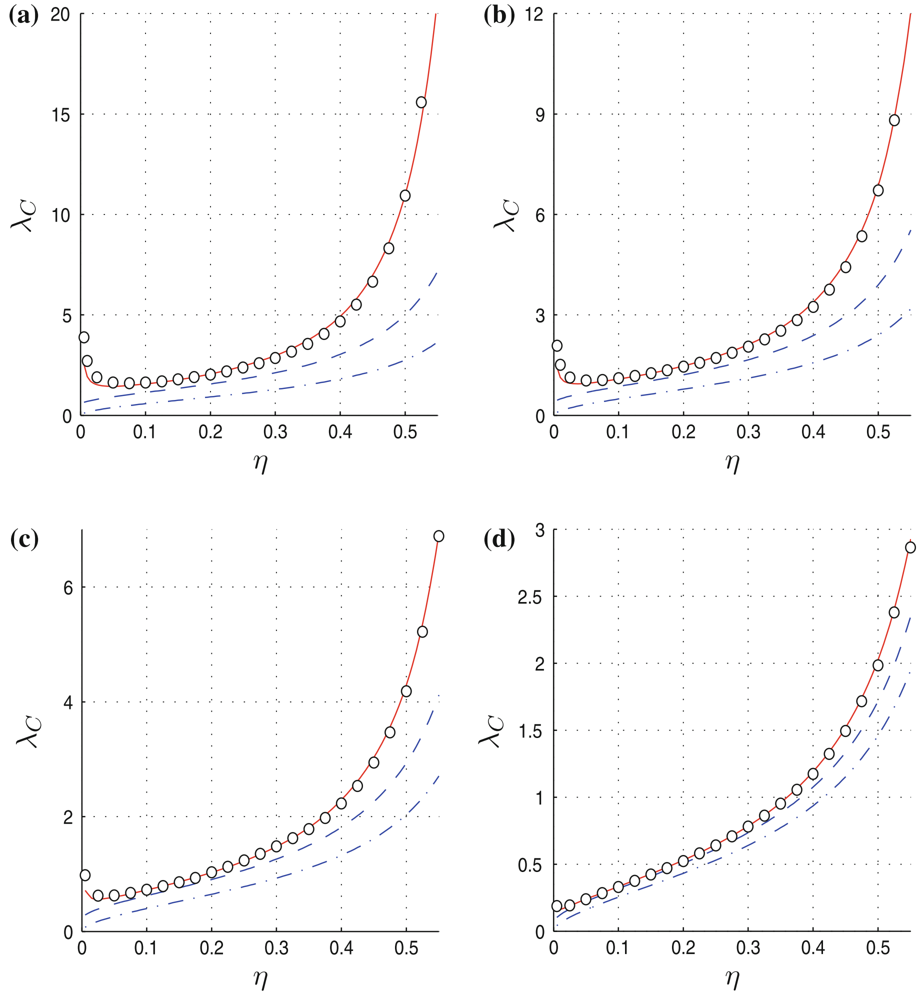

Fig. 9. Same as per Fig. 8, except that $\mu = 40.0$ in (**a**), $\mu = 60.0$ in (**b**), $\mu = 100.0$ in (**c**), and $\mu = 350.0$ in (**d**)

Table 3. *Comparisons between various approximations of the critical eigenvalues and direct numerical simulations (NUM) for the edge-buckling of a clamped rectangular plate. The following conventions are used: ASY II represents the asymptotic result* $\lambda_C := \lambda_0 + \lambda_1^* \mu^{-1/2} + \lambda_2^* \mu^{-1}$ *from the paper [4];* W_0 *denotes the values of* λ *obtained via the modified energy method with the simplest ansatz* $W = W_0$*; finally,* $\widehat{W}$ *is used to identify the approximate eigenvalues obtained with the test function (42). The relative errors (R.E.) with respect to the corresponding direct numerical results are recorded in the last three columns*

μ	NUM	ASY (II)	W_0	$\widehat{W}$	R.E. ASY (II) (%)	R.E. W_0 (%)	R.E. $\widehat{W}$ (%)
10.0	1.226536	0.676648	1.348720	1.329550	44.8326	9.9617	8.3988
20.0	0.620428	0.472876	0.593808	0.617041	23.7824	4.2906	0.5460
30.0	0.468225	0.397007	0.448233	0.464508	15.2103	4.2696	0.7939
40.0	0.399122	0.355988	0.384502	0.396310	10.8073	3.6630	0.7045
50.0	0.359254	0.329800	0.347982	0.357133	8.1988	3.1377	0.5904
100.0	0.280448	0.271139	0.275470	0.279756	3.3196	1.7751	0.2470
200.0	0.238152	0.235099	0.235919	0.237944	1.2819	0.9377	0.0873
300.0	0.222183	0.220574	0.220768	0.222085	0.7244	0.6367	0.0443
400.0	0.213362	0.212336	0.212333	0.213306	0.4809	0.4821	0.0263

interesting to explore the validity of this statement to problems in which the asymptotics are governed by differential equations that are not solvable in closed form. A pertinent example is provided by the paper [25], in which the authors used finite element simulations to identify the optimal choice of such an ansatz. The alternative asymptotic description given by the first author in [20] for the same problem hinged upon a boundary-layer analysis governed by a fourth-order differential equation with variable coefficients. Extending the present work to that situation would be an interesting exercise that we hope to revisit elsewhere.

Acknowledgments

This work was supported by the Engineering and Physical Sciences Research Council through grant EP/F035136. The second author acknowledges with gratitude this financial support through a Studentship, and he would also like to thank the University of Glasgow for some additional financial aid. We thank the anonymous referee for his careful reading of the manuscript.

References

1. Brush, D.O., Almroth, Bo.O.: Buckling of Bars, Plates and Shells. McGraw-Hill, New York (1975)
2. Timoshenko, S.P., Gere, J.M.: Theory of Elastic Stability. McGraw Hill, New York (1961)
3. Coman, C.D.: Edge-buckling in stretched thin films under in-plane bending. Z. Angew. Math. Phys. **58**, 510–525 (2007)
4. Coman, C.D., Bassom, A.P.: Higher-order asymptotics for edge-buckling of pre-stressed thin plates under in-plane bending. J. Eng. Math. **63**, 327–338 (2009)
5. Coman, C.D., Haughton, D.M.: Localised wrinkling instabilities in radially stretched annular thin films. Acta Mech. **185**, 179–200 (2006)
6. Coman, C.D., Bassom, A.P.: On the wrinkling of a pre-stressed annular thin film in tension. J. Mech. Phys. Solids **55**, 1601–1617 (2007)
7. Andersen, C.M., Geer, J.F.: Investigating a hybrid perturbation-Galerkin technique using computer algebra. J. Symb. Comput. **12**, 695–714 (1991)
8. Geer, J.F., Andersen, C.M.: A hybrid perturbation Galerkin technique with applications to slender body theory. SIAM J. Appl. Math. **49**, 344–361 (1989)
9. Geer, J.F., Andersen, C.M.: A hybrid perturbation-Galerkin technique that combines multiple expansions. SIAM J. Appl. Math. **49**, 1474–1495 (1990)
10. Gristchak, V.Z., Dmitrijeva, Ye.M.: A hybrid WKB Galerkin method and its application. Tech. Mech. **15**, 281–294 (1995)
11. Gristchak, V.Z., Ganilova, O.A.: A hybrid WKB-Galerkin method applied to a piezoelectric sandwich plate vibration problem considering shear force effects. J. Sound Vib. **317**, 366–377 (2008)
12. Whitting, A.I.M.: A Galerkin procedure for localised buckling of a strut on a nonlinear elastic foundation. Int. J. Solids Struct. **34**, 727–739 (1977)
13. Wadee, M.K., Coman, C.D., Bassom, A.P.: Numerical stability criteria for localised post-buckling solutions in a strut-on-foundation model. ASME J. Appl. Mech. **71**, 334–341 (2004)
14. Leipholz, H.: Stability Theory. 2nd edn. B.G. Teubner, Stuttgart (1987)
15. Ventsel, E., Krauthammer, T.: Thin Plates and Shells: Theory and Applications. Marcel Dekker, New York (2001)
16. Di Prima, R.C.: Application of the Galerkin method to problems in hydrodynamic stability. Quart. Appl. Math. **13**, 55–62 (1955)
17. Albright, J.R.: Integrals of products of Airy functions. J. Math. Phys. A **10**, 485–490 (1977)
18. Press, W.H., Flannery, B.P., Teukolsky, S.A., Vetterling, W.T.: Numerical Recipies in Fortran: The Art of Scientific Computing. Cambridge University Press, Cambridge (1992)
19. Liu, X.: Boundary eigenvalue problems for elastic instabilities in tension. PhD Thesis, University of Glasgow (2012)
20. Coman, C.D.: Edge-wave buckling of rolled elastic strips: asymptotic results. Acta Mech. **211**, 101–113 (2010)
21. Coman, C.D., Bassom, A.P.: An asymptotic description of the elastic instability of twisted thin elastic plates. Acta Mech. **200**, 59–68 (2008)
22. Coman, C.D., Bassom, A.P.: Erratum to "On the wrinkling of a pre-stressed annular thin film in tension [Journal of the Mechanics and Physics of Solids (2007) 1601]". J. Mech. Phys. Solids **60**, 1240–1240 (2012)
23. Coman, C.D.: Multiple boundary-layer phenomena in the neutral stability envelope of a wrinkling problem. (Unpublished manuscript, 2009)

24. Movchan, A.B., Movchan, A.N.: Mathematical Modelling of Solids with Non-Regular Boundaries. CRC Press, Boca Raton (1995)
25. Rammerstorfer, F.G., Fischer, F.D., Friedl, N.: Buckling of free infinite strips under residual stresses and global tension. ASME J. Appl. Mech. **68**, 804–809 (2001)

Ciprian D. Coman and Xiang Liu
School of Mathematics and Statistics
University of Glasgow
15 University Gardens
Glasgow
G12 8QW
Scotland
UK
e-mail: cdc@maths.gla.ac.uk

(Received: February 20, 2012; revised: May 18, 2012)